Journal of Ceramic Processing Research. Vol. 17, No. 3, pp. 235~239 (2016)

J O U R N A L O F
Ceramic Processing Research

Sonochemical synthesis, characterization, and photocatalytic activities of $PbMoO_4$ photocatalyst

Gobinda Gyawali, Bhupendra Joshi and Soo Wohn Lee*
Research Center for Eco Multi-Functional Nano Materials, Sun Moon University, Asan, Korea

$PbMoO_4$ photocatalysts were synthesized by the facile sonochemical method at 20 kHz frequency with the variable ultrasonic powers, and the results were compared with the sample prepared by conventional co-precipitate method. The synthesized powders were characterized by X-ray Diffraction (XRD) Spectroscopy, X-ray Photoelectron Spectroscopy (XPS), Scanning Electron Microscopy (SEM), and Diffuse Reflectance Spectroscopy (UV-Vis DRS) to investigate the crystal structure, elemental composition, morphology, and optical properties of the photocatalyst. Photocatalytic activities of the $PbMoO_4$ samples were evaluated by the degradation of Methylene Blue (MB), and Indigo Carmine (IC) dyes under UV irradiation. It has been observed that the photocatalyst sample prepared by the sonochemical method at an ultrasonic power of 600 W showed the enhanced photocatalytic performance towards the dyes degradation.

Key words: $PbMoO_4$, Scheelite, Photocatalyst, Co-precipitation, Ultrasound.

Introduction

Photocatalytic degradation of organic pollutants by semiconductor materials has attracted much attention in recent years because the technique is simple and efficient for the removal of organic pollutants [1, 2]. The scheelite structured ternary compounds, which belong to the tungstate family, such as $PbMoO_4$, $CaMoO_4$, $BaMoO_4$, $SrMoO_4$ etc., have been studied in the past as the potential materials for photoluminescence, solid state lasers, optical fibers, scintillating materials, magnetic materials, sensor materials, etc. [3, 4]. Recently, it has been investigated that some of these tungstate family compounds show their attractive photocatalytic activity for the degradation of organic pollutants despite of their relatively larger band-gap energies [5, 6]. Studies on electronic structures and photocatalytic activities of $PbMoO_4$ have revealed that the valence band of $PbMoO_4$ consists of the hybrid orbitals of O2p as well as Pb6s and the conduction band consists of Mo4d orbital and the band gap energy between them is ~3.3 eV [7, 8]. Several synthesis routes have already been proposed in the past for the synthesis of $PbMoO_4$ including chemical precipitation, hydrothermal/solvothermal, microwave, etc. [9, 10]. However, very few investigations have been reported for a sonochemical method and the effects of ultrasonic parameters, such as ultrasonic frequency and powers, on the properties of $PbMoO_4$ photocatalyst [11]. The physical phenomenon responsible for the ultrasonic process is acoustic cavitation. The ultrasonic cavitation generates a very strong stirring environment. Therefore, application of ultrasound is expanding in material science for dispersion, emulsifying, crushing, impregnation, surface treatment, synthesis and activation of nanoparticles. During the process, the rapid ultrasonic vibrations and cavitation effects cause to increase collision between the molecules which in turn enhance the chemical reactivity [12-14]. Hence, ultrasonic frequency and power play a vital role for the variation of morphology and crystallinity of the products.

Therefore, in this article we have reported the synthesis and characterization of $PbMoO_4$ photocatalyst at different ultrasonic powers. The photocatalytic activities of $PbMoO_4$ were systematically evaluated regarding the degradation of aqueous MB and IC dyes under UV light irradiation.

Experimental

Lead Nitrate ($Pb(NO_3)_2$), and Molybdic Acid (H_2MoO_4) were used as the precursor materials to synthesize $PbMoO_4$. All the chemicals were of analytical grade and were used without further purification. Double distilled water was used for all synthesis and treatment processes. First, 4.51 g of $Pb(NO_3)_2$ and 2.20 g of H_2MoO_4 were dissolved separately in 100 mL of double distilled water in two separate beakers. An aqueous solution of $Pb(NO_3)_2$ was then added drop-wise to the beaker containing H_2MoO_4 solution with constant stirring using a magnetic stirrer. The pH of the mixture solution was adjusted to 10 with NH_4OH and HNO_3. The resulting mixture was then transferred to the ultrasonic reactor (SUS304, Asia sonication Ltd.). The ultrasonic frequency was set to 20 kHz and variable

*Corresponding author:
Tel : +82-41-530-2882
Fax: +82-41-530-2840
E-mail: swlee@sunmoon.ac.kr

powers of 600, 800, and 1000 W were adjusted for 2 h. For the comparison purpose, $PbMoO_4$ sample was prepared by co-precipitation method without any ultrasonic treatment. The resulting products were then washed with distilled water and finally with ethanol. The product obtained in this way was air dried at 70 °C for 24 h to remove moisture. The synthesized samples were annealed at 400 °C for 5 h before further characterization. For convenience, the ultrasonic treated $PbMoO_4$ samples at different ultrasonic powers, i.e. 600 W, 800 W and 1000 W were symbolized as LM-06, LM-08, and LM-1, respectively. In the similar manner, the $PbMoO_4$ sample prepared by co-precipitation method was named as LM-C.

Crystalline structure of the catalysts was characterized by XRD with the scanning rate of 4 per minute in a range from 5 to 70 ° using monochromatized Cu Kα (λ = 1.54 Å) radiation (Rigaku X-Ray Diffractometer, Japan). Morphology and particle size of the photocatalysts were analyzed by SEM (Nanoeye). UV-Vis Diffuse Reflectance Spectra were recorded by using UV-Vis spectrophotometer (NIR JASCO 570). XPS measurement was performed by PHI 5000 C ESCA system with MgKα source operating at 14.0 kV and 25 mA. All the binding energies were referenced to the C 1s peak at 284.6 eV. Photocatalytic performance of $PbMoO_4$ (0.1 g catalyst) was evaluated with reference to MB (50 mL of 20 ppm), and IC (50 mL of 20 ppm) dyes degradation in a photoreactor by using UV light irradiation and UV-Vis spectrophotometer (optizen view, Mecasys).

Results and Discussion

XRD analysis was performed to study the crystal structure of the as synthesized samples. Fig. 1 shows the XRD patterns of the samples. From Fig. 1, it is evident that all the diffraction peaks are well indexed to a tetragonal Scheelite structure of $PbMoO_4$ (JCPDS card number 74-1075). The profiles of diffraction peaks in all samples indicate that the powders are well

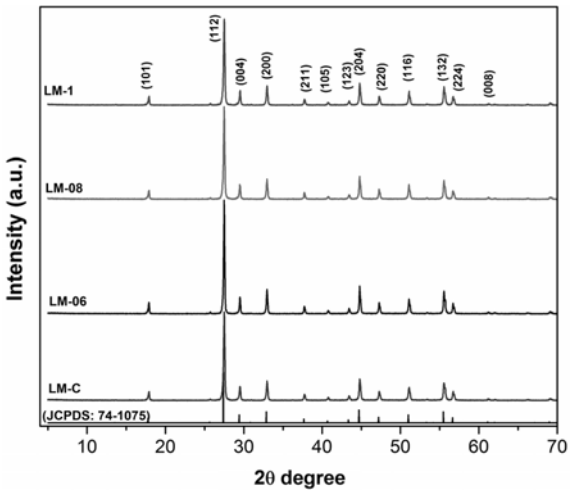

Fig. 1. XRD patterns of the $PbMoO_4$ samples.

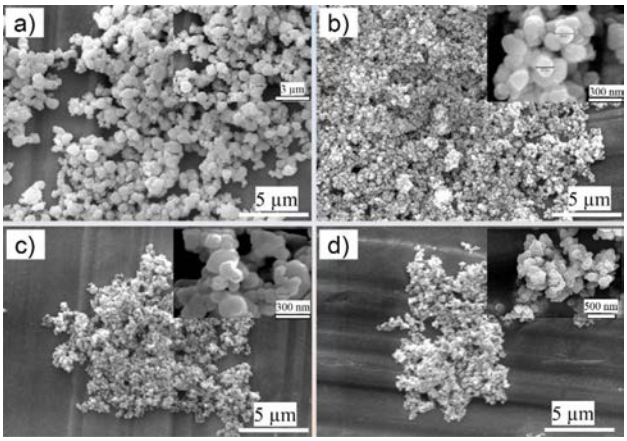

Fig. 2. SEM micrographs of $PbMoO_4$ powders; a) LM-06, b) LM-08, c) LM-1, and d) LM-C samples.

crystallized, and samples contain only $PbMoO_4$ particles, and no additional peaks appeared for any other associated impurities.

Fig. 2 shows the SEM micrographs of the $PbMoO_4$ samples synthesized by co-precipitation method and sonochemical method at different ultrasonic powers. It is interesting to note that the sample LM-06 prepared at 600 W ultrasonic power has shown well crystallized particles with relatively larger and heterogeneously distributed particles in comparison to other specimens. As the ultrasonic powers increased to 800 W and 1000 W, relatively very smaller sized $PbMoO_4$ particles are formed. Such decrease in particles size is due to the increased cavitation effect and crushing of the particles at higher ultrasonic power. The average particles size of $PbMoO_4$ prepared at 1000 W is about 100 nm that is smaller in comparison to the 160 nm average particles size of the sample prepared at 800 W power. Furthermore, there is nearly a homogeneous distribution of particles with spherical shape at such high power of ultrasonically treated samples. On the other hand, a wide distribution of particles size ranging from 160 nm to about 1.4 μm is clearly observed in the sample prepared at 600 W ultrasonic power under constant 20 kHz ultrasonic frequency. Such a wide distribution of particles with different morphologies at 600 W ultrasonic power is mainly due to the lower cavitation and crushing effects of ultrasound. Shen *et al.* [15] obtained the (001) facet $PbMoO_4$ microcrystal under controlled hydrothermal treatment by application of CTAB. The evolution of anisotropic growth and a number of facet polyhedron particles were also observed. Furthermore, enhanced photocatalytic activities were also observed for facet $PbMoO_4$.

Compositional analysis and chemical states of the components present in the photocatalyst have been investigated by XPS analysis. Fig. 3a shows the XPS survey scan of the LM-06 sample. It is clear from the spectrum that the $PbMoO_4$ photocatalyst consists of Pb, Mo, and O elements and no any other impurity peaks

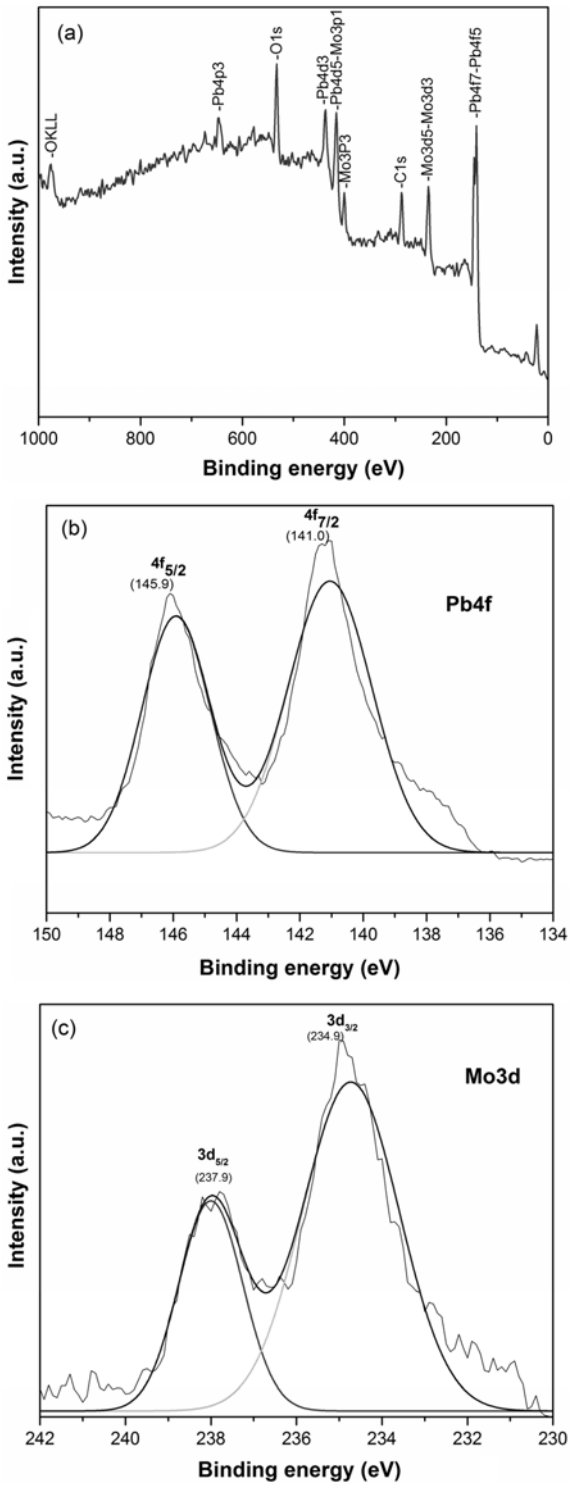

Fig. 3. XPS spectra of LM-06 sample; a) general survey spectrum of $PbMoO_4$, b) high resolution spectrum of Pb4f region and c) high resolution spectrum of Mo3d region.

detected. The high resolution XPS spectra in the Pb4f region of $PbMoO_4$ is shown in Fig. 3b. The peaks at 145.9 and 141.0 eV are ascribed to PbO, which is originated from Pb^{M+} ion of $PbMoO_4$ [16]. Similarly, Mo3d peaks at 237.9 eV and 234.9 eV which are originated from the Mo^{n+} states of MoO_3, and the

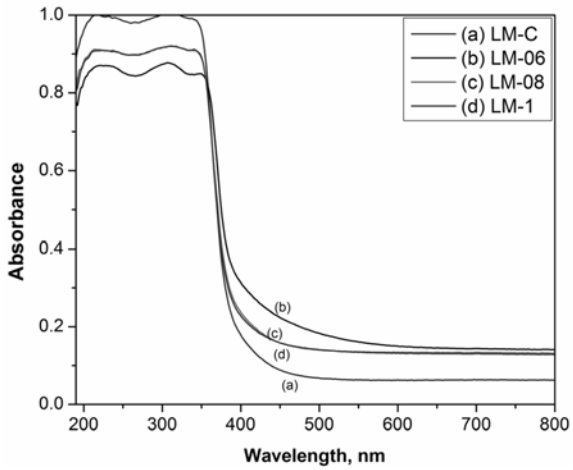

Fig. 4. UV-vis DRS spectra of different $PbMoO_4$ samples.

splitting of the 3d doublet (3d3/2) is approximately at 3.0 eV [17,18] as shown in Fig. 3c. Hence, from XPS analysis it can be stated that the photocatalyst consists principally of Pb, Mo, and O constituents.

UV-vis diffuse reflectance spectra of the different $PbMoO_4$ samples are shown in Fig. 4. It is observed that the base absorptions of $PbMoO_4$ samples prepared under ultrasonic environment are higher in comparison to the co-precipitated $PbMoO_4$ sample. Similarly, the absorption edge is also slightly shifted towards the longer wavelengths indicating more absorption of light compared to the co-ppt $PbMoO_4$ sample. Also, LM-06 sample shows even higher absorption edge in comparison to LM-08 and LM-1 samples. This outcome is attributed due to the structural and morphological variations in the samples. As it has already been discussed above, the LM-06 sample shows well defined facet structure while the other samples have spherical morphology. The band gap energy was calculated from the modified plot of the Kubelka-Munk function, F(R) versus Energy (eV). The band gap energy of 3.23 eV, 3.27 eV, 3.27 eV and 3.3 eV are obtained for LM-06, LM-08, LM-1 and LM-C samples, respectively. The lowest band gap energy (3.23 eV) is obtained in LM-06 sample whereas the highest band gap energy (3.3 eV) is found for LM-C sample.

In order to evaluate the photocatalytic activity of $PbMoO_4$ samples prepared by the sonochemical method and co-precipitation method, the photocatalytic degradations of MB and IC dyes were carried out in aqueous dispersions under UV light irradiation. As mentioned above, the valence band of $PbMoO_4$ consists of the hybrid orbitals of O2p as well as Pb6s, and the conduction band consists of Mo4d orbital. The calculated band gap energies of our $PbMoO_4$ samples are in the range between 3.23 to 3.3 eV. This band gap energy of $PbMoO_4$ suggests that the photocatalyst $PbMoO_4$ is normally active under UV light. Hence, the photocatalytic activities of the different samples were

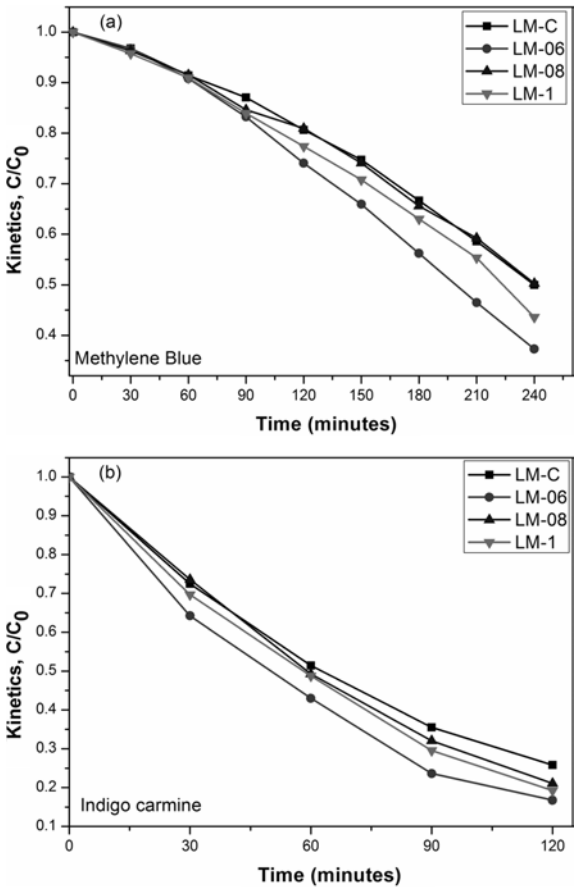

Fig. 5. Kinetics (C/C_0) of the photocatalytic degradation of; a) methylene blue and b) indigo carmine dyes by as synthesized $PbMoO_4$ photocatalysts under UV light irradiation.

evaluated in UV light irradiation under identical conditions. The photocatalytic degradation of aqueous MB and IC dyes solutions under UV light, in terms of kinetic plot (C/C_0), is presented in Fig. 5a and 5b. The intrinsic kinetic parameters of photocatalytic reactions also depend on the optical properties of the photocatalysts in the suspension [11]. In the present work, photocatalytic activity was performed by making a thin film of photocatalyst coating on the bottom of the cell reactor. The negligible adsorption of IC and MB dyes by $PbMOO_4$ photocatalysts were observed during the dark test for initial 1 h. The photocatalytic performance of the $PbMoO_4$ sample synthesized at 600 W ultrasonic power has shown the enhanced photocatalytic activities over other samples for both IC and MB dyes. This result is also ascribed by the relatively higher light absorption profile of the sample in UV-vis DRS spectrum (Fig. 4). Furthermore, the physical properties of the catalyst such as crystalline structure, heterogeneously distributed particles, low charge recombination, and morphology are also known to determine its photocatalytic efficiency in addition to the surface area and particle size of the photocatalysts. The kinetics plot (C/C_0) shows that the photocatalytic activity of $PbMoO_4$ catalyst on indigo carmine dye is higher in comparison to the cationic dye such as methylene blue.

Conclusions

$PbMoO_4$ was successfully synthesized by co-precipitation and sonochemical method with different ultrasonic powers. XRD observation revealed the good crystallinity of the prepared samples without any associated impurities. Increasing the ultrasonic powers resulted the $PbMoO_4$ particles with smaller particles size due to crushing effect of high cavitation energy. The sample prepared at 20 kHz frequency, and the lower ultrasonic power of 600 W has shown the relatively larger but the well crystallized and distinct tetragonal shape of the particles. In addition, the sample showed the enhanced photocatalytic activity towards the degradation of MB and IC dyes. The photocatalytic activity of $PbMoO_4$ on IC dye is observed to be higher in comparison to the MB dye.

Acknowledgments

This research was supported by the Global Research Lab. Program of the National Research Foundation of Korea (NRF) funded by the Ministry of Education, Science and Technology (MEST) of Korea (Grant number: 2010-00339).

References

1. R. Adhikari, S. Malla, G. Gyawali, T.Sekino, S. W. Lee, Mater. Res. Bulletin 48 (2013) 3367-3373.
2. A. Kudo, M. Steinberg, A.J. Bard, A. Campion, M.A. Fox, T.E. Mallouk, S.E. Webber, J.M. White, Catal. Lett. 5 (1990) 61-66.
3. F.B. Cao, L.S. Li, Y.W. Tian, Y.J. Chen, X.R. Wu, Thin Solid Films, 519 (2011) 7971-7976.
4. H. He, J. Huang, L. Cao, X. Ao, Adv. Natur. Appl. Sci. 3 (2009) 204-210.
5. Z. Shan, Y. Wang, H. Ding, F. Huang, J. Mol. Cataly. A, Chem. 302 (2009) 54-58.
6. G.-J. Xing, R. Liu, C. Zhao, Y.-L. Li, Y. Wang, G.-M. Wu, Ceram. Int. 37 (2011) 2951-2956.
7. J. Bi, L. Wu, Y. Zhang, Z. Li, J. Li, X. Fu, Appl. Catal., B 91 (2009) 135-143.
8. Y. Shimodaira, H. Kato, H. Kobayashi, A. Kudo, Bull. Chem. Soc. Jpn. 80 (2007) 885-893.
9. D.B. Hernandez-Uresti, l.C.A. Martinez-de, L.M. Torres-Martinez, , Res. Chem. Interm. 38 (2012) 817-828.
10. D.B. Hernández-Uresti, A. Martínez-de la Cruz, J.A. Aguilar-Garib, Catal.Today 212 (2013) 70-74.
11. G. Gyawali, R. Adhikari, B. Joshi, T.H. Kim, V. Rodríguez-González, S.W. Lee, J. Hazard. Mater. 263 (2013) 45-51.
12. S. Anandan, M. Ashokkumar, Ultrason. Sonochem. 16 (2009) 316-320.
13. T.-H. Kim, V. Rodríguez-González, G. Gyawali, S.-H. Cho, T. Sekino, S.-W. Lee, Catal. Today 212 (2013) 75-80.
14. S.W. Lee, S. Obregón-Alfaro, V. Rodríguez-González, J.

Photochem. Photobiol. A: Chem. 221 (2011) 71-76.
15. M. Shen, Q. Zhang, H. Chen, T. Peng, CrystEngComm. 13 (2011) 2785-2791.
16. M. Milanova, R. Iordanova, K.L. Kostov, J. Non-Crystalline Solids 355 (2009) 379-385.
17. X. Cui, S.H. Yu, L. Li, L. Biao, H. Li, M. Mo, X.M. Liu, Chem. Eur. J. 10 (2004) 218-223.
18. H. Chu, X. Li, G. Chen, Z. Jin, Y. Zhang, Y. Li, Nano Research 1 (2008) 213-220.